SpectralTiming Evolution of a Black hole X-ray binary Swift J1727.81613: Linking Disk Reflection and Type-C QPO Frequency During the 2023 Outburst

Manoj Ghising^a, Nirpat Subba^{b,1,*}, Mohammed Tobrej^a, Binay Rai^a, Bikash Chandra Paul^a

^aNorth Bengal University, Siliguri, Darjeeling, West Bengal, 734013, India ^bCooch Behar Panchanan Barma University, Cooch Behar, West Bengal, 736101, India

We present a comprehensive spectraltiming analysis of a BHXB Swift J1727.8−1613 during its 2023 outburst, using five pointed NaSTAR observations sampling the luminous hardintermediate state. Broadband 379 keV spectroscopy employs a physically motivated model combining a cool truncated disk (diskbb), relativistic reflection (re1x111 in reflection—only mode), and Comptonized continuum (nth/Compt) to probe the inner accretion geometry around a rapidly spinning black hole (a. = 0.98) at moderate inclination. Simultaneous timing analysis reveals type-C quasi-periodic oscillations (QPOs) with novel coherence evolution: the quality factor (Q) exhibits a striking non-monotonic dependence on both QPO frequency and luminosity, peaking near v_{QPO} ~ 1.2 Hz and declining at both lower and higher frequencies. This turnover directly constrains LenseThirring precession geometry, implying optimal coherence at intermediate truncation radius. A tight photon-indexQPO-frequency correlation demonstrates that spectral soft in glisk and Compton, declining reflectiontraces precession-driven geometry changes and corona beaming effects. Interpreting disk-normalization variability as apparent-area changes rather than physical radius swings provides new insight into disk-corona and spectral properties, establishing Swift J1727.8−1613 as a benchmark source for understanding accretion-geometry physics during black hole state transitions.

1. Introduction

1. Introduction

1. Introduction

2. Introduction

3. Introduction

3. Introduction

4. Introduction

3. Introduction

4. Introduction

4. Introduction

4. Introduction

5. Introduction

5. Introduction

6. Introduction

7. Introduction

8. A consolidated phenomenology partitions (LFQPOs) are the around the propertion of the propertion of the propertion o

strong and coherent (up to $\sim 16\%$ rms with $Q \sim 712$), occur at ~0.115 Hz, and commonly exhibit subharmonic and secondharmonic peaks on top of flattop noise; their rms typically rises with photon energy and saturates above ~10 keV. Type B QPOs are narrower, cluster near ~6 Hz, and are associated with weaker noise; abrupt appearances/disappearances are often observed close to state transitions. Type A features are broader

Email address: nirpat.subba@gmail.com()

softer values as the centroid frequency increases, and harmonicdependent behaviour is common (soft at the subharmonic; hard at the second harmonic). Together with the rmsenergy rise and highenergy flattening, these properties implicate a Comptonizing region as the principal variable component and motivate models invoking geometric precession, oscillatory coronae, or instabilitydriven variability. In practice, the LFQPO taxonomy and its placement in the hardnessintensity diagram provide an observational scaffold for linking timing signals to changing accretionflow structure and for benchmarking theoretical interpretations in newly discovered BH transients (Ingram

^{*}Corresponding author

¹ORCID: 0000-0001-7136-7270

and Motta, 2020; Casella et al., 2005).

The 20232024 outburst of a BHXB Swift J1727.8-1613 immediately triggered multi-mission coverage from various observatories. During the onset of the outburst, IXPE measured a linear X-ray polarization of the source to be ~4% with a stable polarization angle in the bright hard stateevidence for an elongated, anisotropic corona oriented roughly orthogonal to the radio jet (Veledina et al., 2023). Concurrent hard-X-ray monitoring through the initial rise and plateau traced a type-C LFQPO and revealed an additional hard tail extending to at least $\gtrsim 400 \text{ keV}$ (Mereminskiy et al., 2024). A coordinated IXPE campaign then followed the source across the hard-soft transition, during which the polarization degree collapsed to $\lesssim 1\%$, demonstrating strong state dependence of the inner-flow geometry (Ingram et al., 2023; Podgorný et al., 2024b). On QPO timescales, polarimetric analyses provided the first constraints on modulation of polarization degree and angle in a BHXB, tying the low-frequency oscillation directly to changes in the emitting geometry (Zhao et al., 2024).

High-resolution radio imaging and monitoring revealed an unusually extended, two-sided, continuous jet with a bright compact core during the hard/hard-intermediate states (Wood et al., 2024), refined by subsequent VLBI imaging at higher resolution (Cao et al., 2025a) and dense radio campaigns mapping the jet evolution and radio-X-ray coupling (Hughes et al., 2025b). Time-dependent visibility modeling of VLBA data resolved multiple transient knots and dated ejections to within tens of minutes, directly associating knot launch with X-ray state/timing changes (Wood et al., 2024). A discrete, rapidly evolving ejection event was further identified in interferometric data (Hughes et al., 2025b). Together with radio/Xray correlation work highlighting the systems peculiar hard state behavior (Hughes et al., 2025a) and jet-extended emission modeling (Zdziarski et al., 2025), these results establish Swift J1727.8-1613 as a premier case for studying compact jets in outbursting BHXBs.

On the X-ray timing/spectral side, multi-mission analyses (NICER, NuSTAR, Insight-HXMT, and AstroSat) tracked the evolution of type-C QPOs across hard and intermediate states, including to ~100 keV (Nandi et al., 2024; Yang et al., 2024). Broadband spectral work during the rising phases showed a weak reflection component plus an extra hard continuum below 100 keV (Liu et al., 2024), while energy-dependent QPO studies revealed frequency and rms trends consistent with geometric precession at high inclination (Zhao et al., 2024; Liao et al., 2025). Phase-resolved spectroscopy demonstrated QPO-phase modulation of the thermal and non-thermal components and reflection fraction (Shui et al., 2024). Detailed spectral-timing modeling of QPO rms/lag spectra captured the radial evolution of the truncation radius and coronal size during the rise (Rawat et al., 2025; Bollemeijer et al., 2025), and cross-spectral analyses uncovered a pronounced dip/negative real-part feature at a few-tens of Hz indicating multiple variability zones in the inner flow (Jin et al., 2025). Flaring episodes during the very high/intermediate states were characterized spectrally and linked to changing disk radius and possible synchrotron self-Compton contributions (Cao et al., 2025b). A soft time lag at

the type-C QPO frequency near outburst peak further supported a high-inclination geometry and strong reverberation (Debnath et al., 2024). Early Insight-HXMT timing already established persistent type-C QPOs and PBK-like correlations (Yu et al., 2024), with additional NICER/NuSTAR/HXMT joint analysis reporting high spin and moderate inclination solutions when including the extra hard component (Peng et al., 2024).

Polarization measurements outside the soft state showed recovery of the hard-state PD/PA after the return to harder spectra (Podgorný et al., 2024c), and soft γ -ray polarization was detected with INTEGRAL/IBIS in both hard-intermediate and early soft-intermediate states, sometimes aligning with the jet (Bouchet et al., 2024). Comparative and review works situate Swift J1727.8–1613 in the broader context of spectropolarimetric state evolution, IXPE advances and source comparisons (Titarchuk et al., 2025; Brigitte and Svoboda, 2025; Ewing et al., 2025).

Dynamical work has now fixed the binary scale. In quiescence, time-resolved optical spectroscopy measured $P_{\rm orb} \approx$ 10.8038 h and $K_2 \simeq 390 \; \text{km s}^{-1}$, yielding $f(M) \approx 2.77 \, M_{\odot}$ and confirming a black-hole primary; the same study refined the distance to 3.7 ± 0.3 kpc (Mata Sánchez et al., 2024). A complementary analysis using H I absorption and reddening argues that somewhat larger distances remain possible (Burridge et al., 2025). Multi-mission timing/spectral papers constrain the truncation of the disc, the size of the Comptonizing region, and the coupling to the compact jet (Majumder et al., 2025; Brigitte et al., 2025; Peng et al., 2025; Debnath et al., 2025). Theory and simulations of disc oscillations and shock-driven instabilities supply a framework consistent with the observed LFQPO energetics and frequencyenergy trends in J1727 (Zhou et al., 2025). Taken togetherpolarimetry across state changes, broadband spectraltiming (including cross-spectral dip behavior), and VLBI-resolved jetsSwift J1727.8-1613 now offers an end-to-end view of accretion-geometry evolution and jet launching in a single, well-observed outburst, providing a stringent benchmark for models of diskcoronajet coupling.

Here, we present a comprehensive spectraltiming investigation of Swift J1727.8–1613's 2023 outburst, examining the coevolution of disk reflection parameters and type-C QPO properties to advance our understanding of black hole accretion dynamics. In this work, we present a comprehensive broadband NuSTAR spectral analysis of Swift J1727.8–1613, employing a physically motivated model combining diskbb, relxill and nthcomp to constrain the system's fundamental parameters during its exceptional 2023 outburst. The list of observations and its exposure corresponding to our BH candidate is shown in Table 1.

2. Data Reduction

2.1. NuSTAR

The BHXB Swift J1727.8–1613 were analyzed by using *NuSTAR* observations during its 2023 outburst as shown in Table 1. It consists of two focal plane modules, FPMA and FPMB that provides simultaneous measurements of X-ray data

Table 1: Details of *NuSTAR* observations of BHXB Swift J1727.8–1613 and its exposure (in ks).

(111 113).		
Date	ObsID	Exposure (ks)
2023-08-29	90902330002	0.92
2023-09-01	80902333002	1.52
2023-09-04	80902333004	1.27
2023-09-07	80902333006	0.67
2023-09-08	80902333008	0.54

in the 379 keV range. The unfiltered event data were processed with mission specific script using NuSTARDAS v2.1.2 and HEASoft v6.35 along with the latest NuSTAR CALDB files. The clean Event datas were extracted with the script nupipeline by applying standard screening criteria. Using XSELECT ftools, cleaned event data were then loaded and extracted. With the help of Astronomical imaging software Ds9, the respective source and background region files were extracted with a circular region of 100" centered on the BH source Swift J1727.8-1613. The background region files were extracted from nearby source-free regions on the same chip. Using the script nuproducts, we generated lightcurve, spectra, response matrices, and ancillary response files in 3-79 keV energy range. Using ftool POWSPEC, we determined the QPO values for each light curve of different observation listed in Table 2. The spectra were grouped to have a minimum of 20 counts per bin using the command GRPPHA. The spectra of the source were then loaded in XSPEC for fitting (Arnaud, 1996).

2.2. Swift/BAT and MAXI

In order to see the daily light curve of the BHXB Swift J1727.8–1613 during 2023 outbursts, we made use of data from the Burst Alert Telescope (BAT) onboard the Neil Gehrels Swift Observatory. The Swift/BAT transient monitor provides daily light curves in the 1550 keV energy band. We retrieved the publicly available BAT light curves from the official HEASARC archive and used them to trace the long-term flux evolution of the source. In addition, soft X-ray monitoring was carried out with the Gas Slit Camera (GSC) onboard the Monitor of All-sky X-ray Image (MAXI) mission. MAXI/GSC provides 220,keV light curves with a typical orbital timescale sampling. The combined BAT and MAXI datasets were used to study the light curve of the source and to identify the epochs corresponding to our pointed NuSTAR observations (see Figure 1.

Table 2: Unabsorbed 0.1100 keV total luminosity (in the scale of 10^{38} erg s⁻¹), QPO centroid frequency ($\nu_{\rm QPO}$), and Quality factor (Q) with uncertainties for 5 NuSTAR observations

Trus TAIX Observations.			
NuSTAR OB IDs	L	$ u_{ m QPO}$	Q
90902330002	6.99 ± 0.005	0.84 ± 0.01	3.13 ± 0.11
80902333002	6.98 ± 0.004	1.22 ± 0.06	3.30 ± 0.09
80902333004	6.77 ± 0.004	1.18 ± 0.04	3.03 ± 0.16
80902333006	7.23 ± 0.007	1.45 ± 0.09	2.08 ± 0.12
80902333008	6.43 ± 0.007	1.30 ± 0.08	1.86 ± 0.13

3. Timing analysis

We performed timing analysis on the 379 keV NuSTAR light curves extracted using the mission specific nuproducts pipeline. Background subtraction was carried out with ftool LCMATH, and barycentric corrections were performed using ftool BARYCORR. Figure 1 shows the MAXI and *Swift/BAT* light curves (Rate vs. time in MJD), with the epochs of NuSTAR observations in our study indicated by vertical lines. Power density spectra (PDS) were produced with POWSPEC using 0.01 s binsize and normalized following the fractional rms convention. Each PDS was fitted with four zero-centered Lorentzians model to represent the broad-band noise, together with a power-law continuum (Figure 2 & 3). An example of the PDS fit is displayed in Figure 2.

We detect a single dominant type-C QPO in all five NuSTAR observations of Swift J1727.8-1613, with centroid frequencies $\nu_{\rm OPO} = 0.84 \pm 0.01, 1.22 \pm 0.06, 1.18 \pm 0.04, 1.42 \pm 0.09,$ and 1.30 ± 0.08 Hz (Table 2), consistent with the timing evolution reported for this source (Yu et al., 2024). Figure 4 shows that the quality factor peaks near $\nu_{\rm OPO} \sim 1.2~{\rm Hz}$ ($Q \approx 3.2 - 3.3$), remains high at 0.84 Hz ($Q \sim 3.1$), and declines to $Q \sim 2.0$ at the highest frequency (~1.45 Hz), revealing a clear turnover rather than a monotonic trend across 0.84-1.45 Hz. An analogous turnover is present versus unabsorbed luminosity: Q is maximal at intermediate $L \approx (6.9-7.0) \times 10^{38} \text{ erg s}^{-1}$ and decreases toward both lower and higher L, implying optimal coherence at moderate accretion rates. This pattern matches expectations of a precessing inner hot flow undergoing Lense-Thirring precession, where coherence is regulated by truncation radius and damping in the inner flow (Ingram et al., 2009; Ingram and van der Klis, 2017; Ingram and Motta, 2019). Comparable behaviorenhanced coherence in the hardintermediate state and weakening as the geometry evolveshas been observed in GX 339-4, supporting a changing truncation radius and precessing inner flow scenario (Fürst et al., 2016).

The combined analysis of the fractional-rms power heat map (Fig. 5) and the two-panel MAXI/GSC and Swift/BAT light curve (Fig. 1) reveals the temporal evolution of variability and flux through the 2023 outburst of Swift J1727.8-1613. During the early hard state, the type-C QPO appears in the ~ 0.8 -1.0 Hz band and strengthens as the source brightens, consistent with NICER and Insight-HXMT monitoring that tracked the rise of the type-C QPO from sub-Hz to a few Hz as hardness decreased (Stiele and Kong, 2024; Yu et al., 2024; Liu et al., 2024). The contemporaneous long-term behaviour seen in the public MAXI/GSC and Swift/BAT monitors shows the outburst rise and subsequent hard-state plateau against which our pointed NuSTAR epochs are marked. Around MJD ~60194 (ObsID 80902333004), the QPO centroid shifts toward ~1.2-1.3 Hz, as expected if the inner hot flow contracts and the Comptonized component strengthens (Yu et al., 2024; Liu et al., 2024; Peng et al., 2024). Entering the hardintermediate state, the broadband fractional rms decreases while the QPO persists at ~1-2 Hz, in line with NICER tracking and broadband studies of this outburst (Stiele and Kong, 2024; Mereminskiy et al., 2024). As the source softens further (post-plateau), the rms

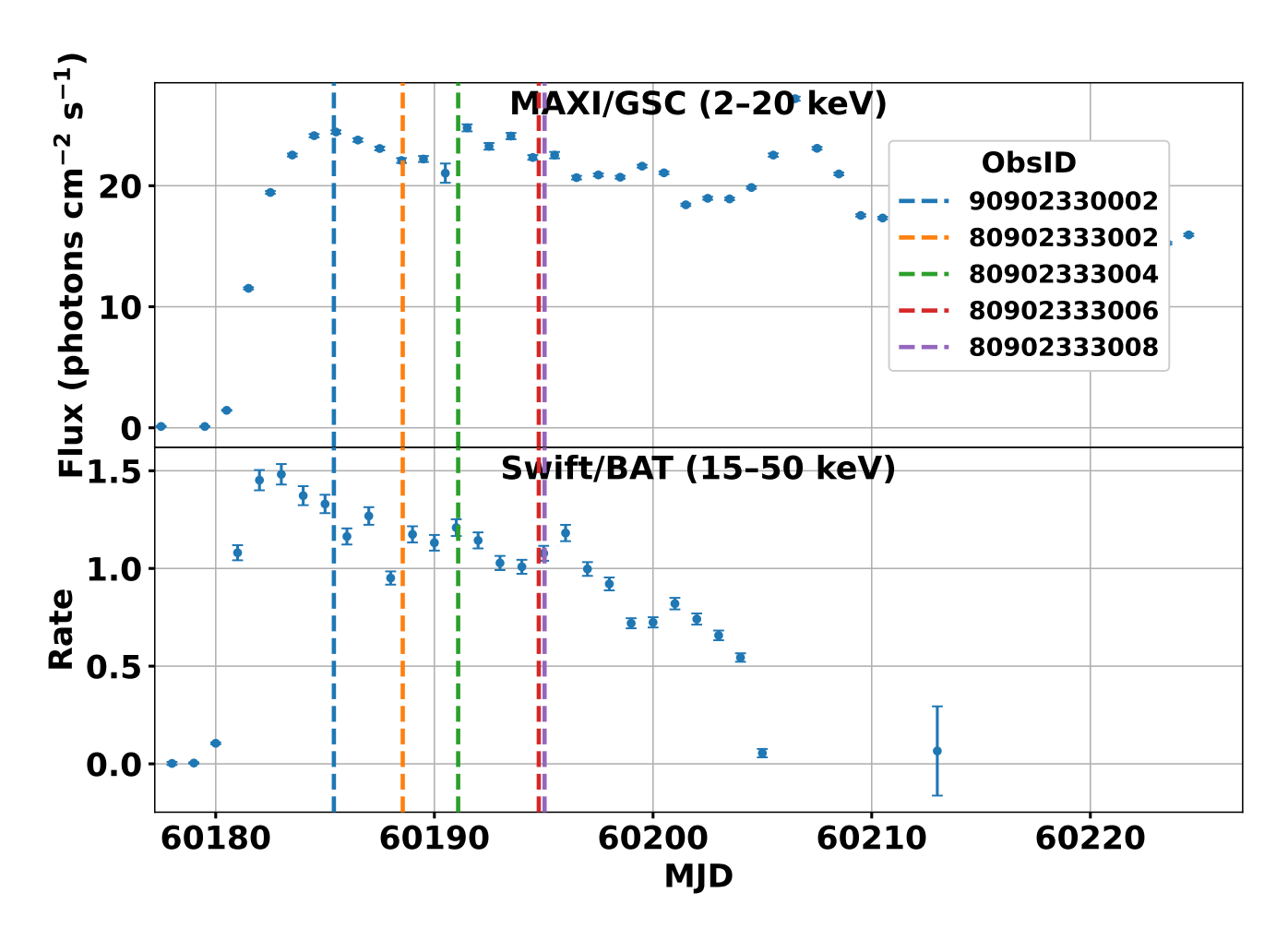


Figure 1: Two-panel light curve centered on the observation epochs: **top-**MAXI/GSC (220 keV) flux (photons cm⁻² s⁻¹) (source link); **bottom-**Swift/BAT (1550 keV) rate (source link). Colored dashed vertical lines mark the observation times (labeled by ObsID in the legend) and are drawn continuously across both panels.

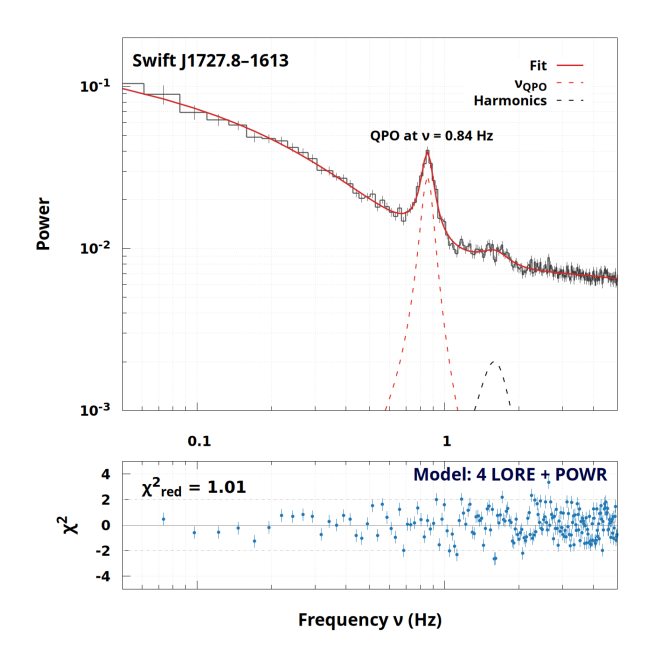


Figure 2: The best-fit power density spectrum (PDS) of Swift J1727.8-1613 in the 3-79 keV energy band from NuSTAR (ObsID: 90902330002) is shown. The PDS is modeled using four Lorentzian components along with a power-law, each representing different features of the variability. The lower panel displays the corresponding residuals.

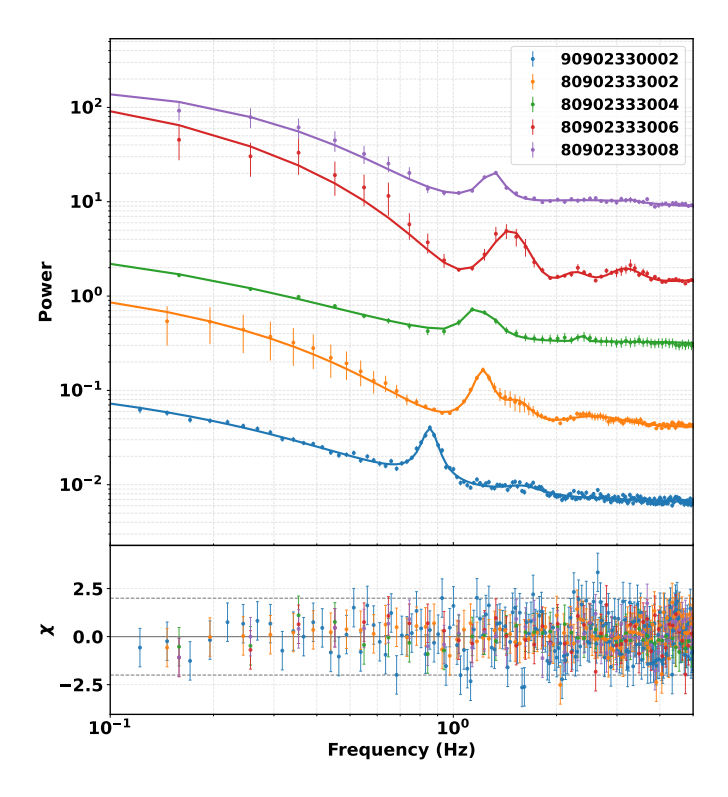


Figure 3: Stacked power spectra of five Swift J1727.8–1613 observations (legend: OBSIDs). Top: data with regenerated best-fit models (constant + power-law continuum + Lorentzian QPO); each spectrum is offset by $\times 10^{\Delta}$ to avoid overlap. Bottom: unstacked residuals.

drops to a few per cent and the type-C feature weakens or disappears, signalling the approach to the soft state (Stiele and Kong, 2024; Liu et al., 2024).

4. Spectral Analysis

379 keV We model the **NuSTAR** spectra constant*TBabs*(diskbb + nthComp + relxill), fixing/tieing parameters to physically motivated values to control degeneracies (Figure 6). Neutral absorption is treated with TBabs using Wilms et al. (2000), fixed at $N_{\rm H} = 0.4 \times 10^{22} \, \rm cm^{-2}$ (Draghis et al., 2023). The FPMA constant is fixed at unity while for FPMB is left free. The disc stays cool and nearly steady, $T_{\rm in} \approx 0.420.51 \,\text{keV}$, while $K_{\rm diskbb} \sim (6.220) \times 10^4 \,\text{(Ta-}$ ble 3). Reflection is described with relxill in reflection only mode (refl_frac=-1), adopting $q_1 = q_2 = 3$, $R_{br} = 15 r_g$, $R_{\rm in} = -1$ (ISCO), $R_{\rm out} = 1000 \, r_g$, $a_* = 0.98$ (Peng et al., 2024), and solar iron. The inclination is moderate and well constrained, $i \sim 45^{\circ}52^{\circ}$. The reflector ionization strengthens toward the middle of the campaign and then relaxes ($\log \xi$ peaking near the central epoch), while the highenergy cutoff increases from \sim 2830 keV to \sim 35 keV later on. The Comptonized continuum (NTHCOMP) shares Γ with RELXILL (tied), adopts $kT_{bb} = T_{in}$, and keeps a lowtomoderate electron temperature $kT_e \sim 1517 \text{ keV}$ (fixed at 16.8 keV in the first epoch where it is unconstrained). The photon index evolves from hard ($\Gamma \approx 1.34$) to softer $(\Gamma \approx 1.54)$ by epoch 4, then slightly decreases to $\Gamma \approx 1.51$ in epoch 5.

Across the five epochs, the unabsorbed luminosity spans $L \simeq 6.437.23 \times 10^{38} \text{ erg s}^{-1}$, enabling a direct comparison of spectral parameters with L (Fig. 7). The disc is cool and only weakly variable, with $T_{\rm in}$ highest near $L \approx 6.986.99 \times 10^{38}$ at $T_{\rm in} \simeq 0.500.51$ keV, cooling to 0.423 keV at the brightest epoch $L \approx 7.23 \times 10^{38}$ before recovering to 0.455 keV at $L \approx 6.43 \times 10^{38}$. The reflector ionization follows the illumination, rising from $\log \xi \simeq 4.024.06$ around $L \approx 6.776.99 \times 10^{38}$ to a peak $\log \xi \simeq 4.18$ at $L \approx 7.23 \times 10^{38}$, remaining elevated at $\log \xi \simeq 4.14$ when the source later dims. The continuum softens with luminosity, with Γ increasing from $\simeq 1.341.42$ near $L \approx 6.986.99 \times 10^{38}$ to $\simeq 1.54$ at $L \approx 7.23 \times 10^{38}$, before settling to $\simeq 1.51$ at $L \approx 6.43 \times 10^{38}$. Consistent with this softening, the electron temperature shows marginal changes with luminosity, cooling from $kT_{\rm e} \simeq 17.1~{\rm keV}$ near $L \approx 6.98 \times 10^{38}$ to $kT_{\rm e} \simeq 14.5~{\rm keV}$ at $L \approx 7.23 \times 10^{38}$, then reheating slightly to $\simeq 16.5~{\rm keV}$ at $L \approx 6.43 \times 10^{38}$. The highenergy cutoff increases from $E_{\rm cut} \simeq 2830 \text{ keV}$ at $L \approx 6.986.99 \times 10^{38} \text{ to} \simeq 35 \text{ keV}$ at $L \approx 7.23 \times 10^{38}$ and remains high thereafter, indicating a brighter yet more optically efficient corona at peak luminosity. As expected for a geometric parameter, the inclination stays consistent within uncertainties at $i \simeq 45^{\circ}52^{\circ}$ with no physical trend versus L.

The QPO centroid increases from ~ 0.84 to ~ 1.45 Hz, accompanied by continuum softening as the photon index rises from ~ 1.34 to ~ 1.54 , indicating a progressively steeper Comptonized tail (Fig. 8). The multicolor disk cools mildly with increasing $\nu_{\rm QPO}$, with $T_{\rm in}$ declining from ~ 0.50 keV at

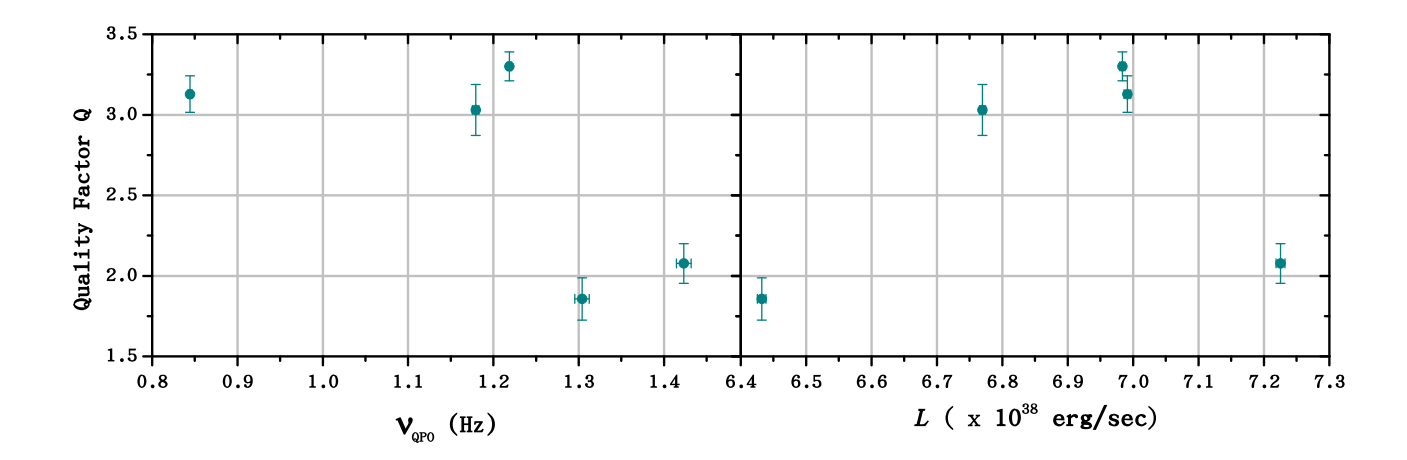


Figure 4: Two-panel comparison of the QPO quality factor. **Left:** Q versus QPO centroid frequency $\nu_{\rm QPO}$. **Right:** Q versus luminosity L. Each point corresponds to one of the five observations, obtained from Lorentzian (LORE) fits to fractional-rms normalized power spectra. The quality factor is defined as $Q \equiv \nu_0/FWHM$. Error bars show 3σ uncertainties.

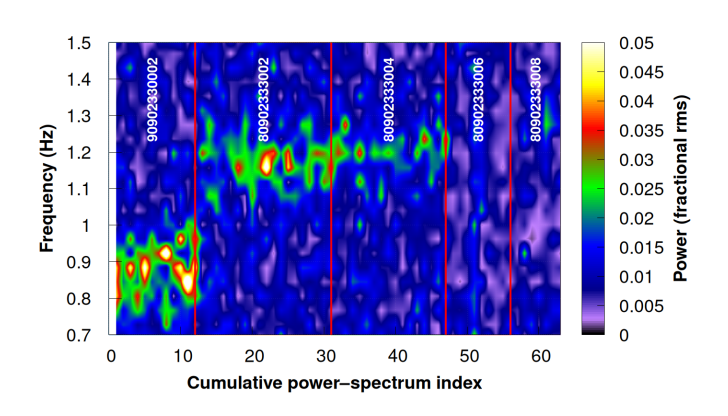


Figure 5: Fractional-rms power heat map for Swift J1727.8-1613: the x-axis is the cumulative power-spectrum index, shaded bands with rotated labels mark each ObsID and thick vertical lines mark their boundaries; the y-axis is frequency (Hz); color encodes fractional-rms power from white (high) to black (low).

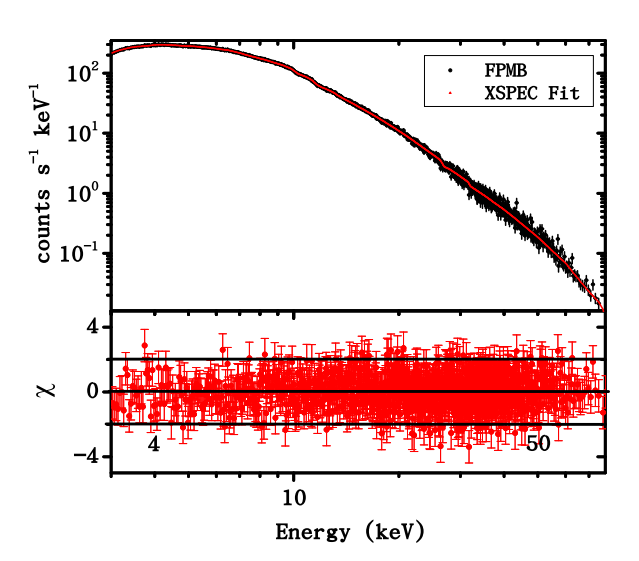


Figure 6: The 3-79 keV spectral fit of NuSTAR FPMB using model combination TBabs*(diskbb+nthComp+relxill)

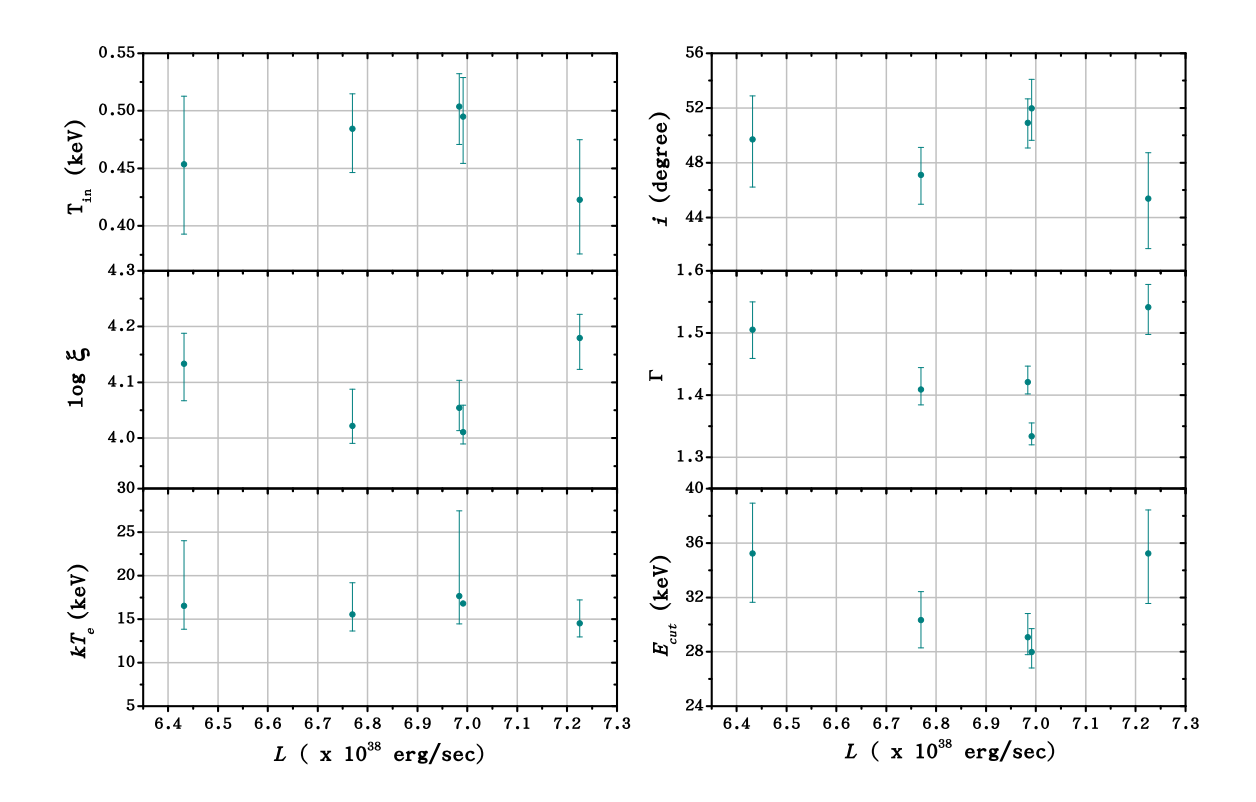


Figure 7: Spectral parameters versus X-ray luminosity L for the five NuSTAR epochs. Left column: inner disc temperature $T_{\rm in}$ (keV), disc ionization $\log(\xi)$, and kT_e . Right column: inclination i (deg), photon index Γ , and cut-off energy (E_{cut}) (keV). The xaxis is L in units of 10^{38} erg s⁻¹ as plotted; points show 3σ errors.

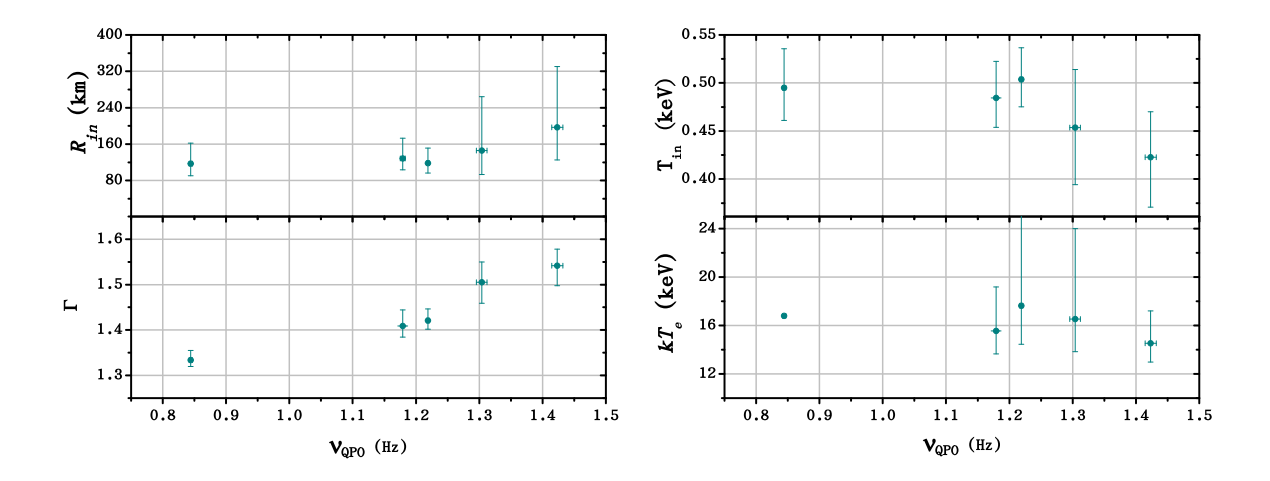


Figure 8: Variation of spectral parameters $R_{\rm in}$, photon index (Γ), inner disc temperature (T_{in}) & kT_e of the BHXB Swift J21727.8-1613 with ν_{QPO} .

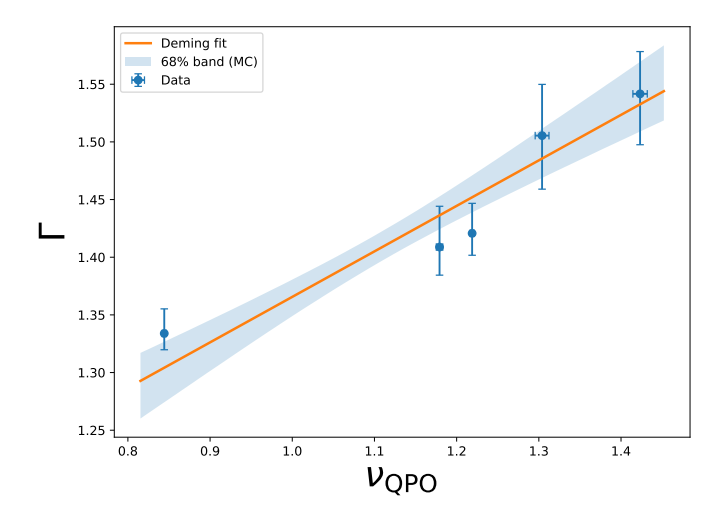


Figure 9: Correlation between QPO frequency $\nu_{\rm QPO}$ (Hz) and photon index Γ with asymmetric 3σ errors. Solid line: Deming fit ($\lambda=0.0323$); shaded band: 68% MC envelope from 5×10^4 resamples. Best-fit: $\Gamma=(0.958^{+0.091}_{-0.102})+(0.408^{+0.091}_{-0.083})\nu_{\rm QPO}$. Pearson r=0.946 (p=0.0083).

the lower- ν_{QPO} epoch to $\approx 0.420.46$ keV at higher ν_{QPO} ; meanwhile, the diskbb normalization is consistent with a larger apparent inner radius, though the trend shows appreciable scatter owing to parameter covariances. The coronal electron temperature remains approximately stable near 15–17 keV without a robust monotonic trend.

5. Discussion

Across the five NuSTAR observations (Table 2), we detect a persistent type-C LFQPO whose centroid energy ranges from $\nu_{\rm OPO} \simeq 0.84 - 1.45$ Hz. The PDS reflects a (Fig. 2) narrow peak with broadband noise that has been modeled by Lorentzian. The prominent feature observed in the PDS represents type-C QPOs generally observed in the hard and hardintermediate states. During the observation period, the source remained near the luminosity plateau (Fig. 1), and the QPO frequency was confined to a relatively narrow band, rather than acquiring higher values observed in other transients during full hard→soft evolution. This behavior is consistent with NICER and InsightHXMT monitoring of the 2023 outburst: NICER observations reveal a rise of the type-C QPO from ~0.32.63 Hz into the few-hertz range as the source softens (Liao et al., 2025; Stiele and Kong, 2024), and HXMT likewise reports type-C QPOs emerging near ~0.7 Hz in the hard state and increasing as the outburst progresses (Liu et al., 2024; Yang et al., 2024). The NuSTAR pointed observations analyzed in the present study lies in the luminous hardintermediate state where the QPO is known to range in the limit ~1 Hz before vanishing as the source completes transition (Stiele and Kong, 2024; Liao et al., 2025).

A key novel element of our timing analysis is the *coherence* (quality factor) evolution across this narrow $v_{\rm QPO}$ range (Fig. 4). We find that Q rises to a maximum $Q \simeq 3.3$ near $v_{\rm QPO} \sim 1.2$ Hz and then declines to $Q \simeq 2.0$ at ~ 1.4 Hz. While type-C QPOs can reach higher Q at lower frequencies in the classical lowhard

state, moderate coherence ($Q \sim 23$) during the bright hardintermediate phase is consistent with hardX-ray timing reports for this outburst (e.g. AstroSat and HXMT) (see Liu et al., 2024; Yang et al., 2024). To our knowledge, a clear non-monotonic Q(v) trend has not been emphasized for Swift J1727.8–1613 in the literature; our result suggests an optimal inner-flow configuration (around ~ 11.2 Hz) where the precession is most coherent, followed by damping as the system approaches the state transition. This is qualitatively compatible with LT-precession frameworks where the coherence depends on geometry, viscous coupling, and the fractional contribution of the precessing flow.

spectroscopy Broadband 3–79 keV *NuSTAR* Swift J1727.8-1613 (Table 3) supports a geometrically stratified accretion picture: a cool, thin disk truncated at the inner stable circular orbit (ISCO) transitions to a geometrically thick, hot inner flow. The disk-corona-reflection geometry, modeled constant*TBabs*(diskbb + relxill + nthComp), places RELXILL in reflection-only mode (refl_frac=-1) with a separate NTHCOMP continuum, a configuration that avoids double-counting of the hard Comptonization and isolates the thermal disk and reflection. By fixing $R_{\rm in}$ to the ISCO in RELXILL, we assume the disk has already receded inward to its theoretical minimum, a picture supported by joint NICER+NuSTAR+HXMT fitting and consistent with a rapidly spinning black hole ($a_* = 0.98$) at moderate inclination $(i \simeq 45^{\circ} - 52^{\circ})$ (Peng et al., 2024; Liu et al., 2024; Ingram et al., 2023; Podgorný et al., 2024a).

The continuum softens progressively as luminosity rises: Γ increases from $\simeq 1.34$ to $\simeq 1.54$ (epoch 4) before settling to $\simeq 1.51$ at the faintest point, consistent with enhanced Compton cooling as the disk seedphoton supply grows. By contrast, the electron temperature shows only marginal evidence for a decrease with luminosity: $kT_e = 17.13^{+7.88}_{-2.91}$, $15.33^{+3.34}_{-1.87}$, $14.52^{+2.60}_{-1.56}$, and $16.45^{+7.16}_{-2.66}$ keV across $L \simeq (6.98, 6.77, 7.23, 6.43) \times 10^{38}$ 10^{38} erg s⁻¹ (epoch 1 fixed at 16.8 keV). Given the overlapping 3σ intervals, a constant $kT_{\rm e}$ in the range ~1517 keV is statistically acceptable, with a shallow minimum near peak L rather than a significant anticorrelation. The cutoff energy increases from $E_{\rm cut} \sim 2830 \text{ keV}$ to $\sim 35 \text{ keV}$ at peak luminosity, indicating a more optically efficient corona at highest L. The reflector ionization tracks illumination, with $\log \xi$ rising from ~ 4.02 to ~ 4.18 and then relaxing to $\sim 4.14.$ The disk temperature remains nearly constant ($T_{\rm in} \approx 0.420.51 \text{ keV}$), while $K_{\rm diskbb}$ varies by a factor ~3, which we interpret as apparentarea or colorcorrection changes rather than large physical radius swings as the coronal geometry evolves.

The quality factor evolution in Figure 4 reveals a striking peak near $\nu_{\rm QPO} \sim 1.2$ Hz ($Q \sim 3.3$) that declines at both lower and higher frequencies, with a turnover to $Q \sim 2.0$ at $\nu_{\rm QPO} \sim 1.45$ Hz. Importantly, this non-monotonic $Q(\nu_{\rm QPO})$ behavior does not appear to be a statistical artifact: within the narrow luminosity band sampled (a factor ~ 1.1 in L), the coherence maximum pins to an intermediate geometry characterized by moderate truncation radius and intermediate accretion rates. In the Lense–Thirring precession framework (Ingram et al., 2009; Ingram and van der Klis, 2017), such a turnover is naturally expected: as the truncation radius sweeps inward, the precess-

Table 3: Bestfit parameters for constant*TBabs*(diskbb + relxill + nthComp) for five NuSTAR observations of Swift J1727.8–1613. Entries are $x_{-\Delta x}^{+\Delta x}$ (3 σ). Parameters marked (fixed) are frozen across all observations; (tied) indicates a parameter tied as noted in the model.

	90902330002	80902333002	80902333004	80902333006	80902333008
Absorption					
$N_{\rm H}~(10^{22}~{\rm cm}^{-2})$	0.4 (fixed)	0.4 (fixed)	0.4 (fixed)	0.4 (fixed)	0.4 (fixed)
diskbb					
$T_{\rm in}~({\rm keV})$	$0.495^{+0.034}_{-0.039}$	$0.505^{+0.030}_{-0.033}$	$0.486^{+0.029}_{-0.038}$	$0.423^{+0.052}_{-0.046}$	$0.455^{+0.059}_{-0.061}$
$K_{\rm diskbb}~(\times 10^4)$	$6.18^{+5.08}_{-2.30}$	$6.46^{+3.72}_{-1.98}$	$8.22^{+6.12}_{-2.66}$	$20^{+32.8}_{-11.4}$	$10.0^{+20.7}_{-5.66}$
relxill					
q_1	3 (fixed)	3 (fixed)	3 (fixed)	3 (fixed)	3 (fixed)
q_2	3 (fixed)	3 (fixed)	3 (fixed)	3 (fixed)	3 (fixed)
$R_{\rm br} \left(r_{\rm g} \right)$	15 (fixed)	15 (fixed)	15 (fixed)	15 (fixed)	15 (fixed)
a_*	0.98 (fixed)	0.98 (fixed)	0.98 (fixed)	0.98 (fixed)	0.98 (fixed)
i (deg)	$51.84^{+2.16}_{-2.41}$	$50.81^{+1.78}_{-1.84}$	$47.03^{+2.01}_{-2.13}$	$45.32^{+3.36}_{-3.64}$	$49.66^{+3.17}_{-3.50}$
$R_{\rm in} (r_{\rm g})$	-1 (fixed)	-1 (fixed)	-1 (fixed)	-1 (fixed)	-1 (fixed)
$R_{\rm out} (r_{\rm g})$	1000 (fixed)	1000 (fixed)	1000 (fixed)	1000 (fixed)	1000 (fixed)
z	0 (fixed)	0 (fixed)	0 (fixed)	0 (fixed)	0 (fixed)
Γ	$1.339^{+0.020}_{-0.014}$	$1.422^{+0.027}_{-0.020}$	$1.411^{+0.036}_{-0.024}$	$1.543^{+0.036}_{-0.043}$	$1.507^{+0.043}_{-0.046}$
$\log \xi$	$4.021^{+0.0444}_{-0.0268}$	$4.060^{+0.0501}_{-0.0428}$	$4.029^{+0.0652}_{-0.0350}$	$4.184^{+0.0412}_{-0.0542}$	$4.139^{+0.0535}_{-0.0651}$
$A_{\rm Fe}$ (solar)	1 (fixed)	1 (fixed)	1 (fixed)	1 (fixed)	1 (fixed)
$E_{\rm cut}$ (keV)	$27.99^{+1.69}_{-1.22}$	$28.78^{+1.84}_{-1.35}$	$30.12^{+2.14}_{-1.85}$	$35.14^{+3.14}_{-3.64}$	$35.03^{+3.69}_{-3.60}$
refl_frac	-1 (fixed)	-1 (fixed)	-1 (fixed)	-1 (fixed)	-1 (fixed)
$K_{\rm relxill}$	$0.483^{+0.00834}_{-0.0164}$	$0.447^{+0.0145}_{-0.0139}$	$0.399^{+0.0136}_{-0.0129}$	$0.362^{+0.0214}_{-0.0194}$	$0.385^{+0.0259}_{-0.0226}$
nthComp					
Γ	(tied to relxill Γ)	(tied)	(tied)	(tied)	(tied)
$kT_{\rm e}$ (keV)	16.8 (fixed)	$17.13^{+7.88}_{-2.91}$	$15.33^{+3.34}_{-1.87}$	$14.52^{+2.60}_{-1.56}$	$16.45^{+7.16}_{-2.66}$
$kT_{\rm bb}$ (keV)	$= T_{\rm in}$ (tied)	(tied)	(tied)	(tied)	(tied)
inp_type	1 (fixed)	1 (fixed)	1 (fixed)	1 (fixed)	1 (fixed)
z	0 (fixed)	0 (fixed)	0 (fixed)	0 (fixed)	0 (fixed)
$K_{ m nthComp}$	$0.291^{+0.0323}_{-0.0236}$	$0.502^{+0.0868}_{-0.0630}$	$0.516^{+0.111}_{-0.0720}$	$1.086^{+0.256}_{-0.213}$	$0.761^{+0.205}_{-0.152}$
Unabsorbed component fluxes					
$F_{\rm diskbb} \ (10^{-8} \ {\rm erg \ cm^{-2} \ s^{-1}})$	$7.73^{+0.22}_{-0.22}$	$8.79^{+0.16}_{-0.16}$	$9.53^{+0.20}_{-0.20}$	$13.30^{+0.49}_{-0.49}$	$8.97^{+0.37}_{-0.37}$
$F_{\text{relxill}} (10^{-8} \text{ erg cm}^{-2} \text{ s}^{-1})$	$32.60^{+0.043}_{-0.044}$	$31.10^{+0.040}_{-0.040}$	$29.00_{-0.041}^{+0.041}$	$27.60^{+0.072}_{-0.072}$	$27.50^{+0.074}_{-0.075}$
$F_{\text{nthComp}} (10^{-8} \text{ erg cm}^{-2} \text{ s}^{-1})$	$2.33^{+0.07}_{-0.07}$	$2.73^{+0.06}_{-0.06}$	$2.82^{+0.06}_{-0.06}$	$3.29^{+0.08}_{-0.08}$	$2.80^{+0.09}_{-0.09}$
Unabsorbed component lumin					
$L_{\rm diskbb}$ (10 ³⁸ erg s ⁻¹)	$1.267^{+0.0361}_{-0.0361}$	$1.439^{+0.0263}_{-0.0263}$	$1.560^{+0.0322}_{-0.0322}$	$2.172^{+0.0802}_{-0.0801}$	$1.469^{+0.0612}_{-0.0610}$
$L_{\text{relxill}} (10^{38} \text{ erg s}^{-1})$	$5.343^{+0.0071}_{-0.0073}$	$5.096^{+0.0066}_{-0.0066}$	$4.748^{+0.0068}_{-0.0068}$	$4.515^{+0.0118}_{-0.0117}$	$4.505^{+0.0120}_{-0.0122}$
$L_{\text{nthComp}} (10^{38} \text{ erg s}^{-1})$	$0.382^{+0.0114}_{-0.0113}$	$0.448^{+0.0092}_{-0.0092}$	$0.461^{+0.0093}_{-0.0092}$	$0.538^{+0.0130}_{-0.0129}$	$0.459^{+0.0147}_{-0.0146}$
Unabsorbed totals		210072	210072	2.07.407	0.0210
$F_{\text{unabs}} (10^{-8} \text{ erg cm}^{-2} \text{ s}^{-1})$	$42.7^{+0.032}_{-0.031}$	$42.6^{+0.025}_{-0.025}$	$41.3^{+0.027}_{-0.028}$	$44.1^{+0.042}_{-0.042}$	$39.3^{+0.042}_{-0.041}$
$L_{\rm unabs} \ (10^{38} \ {\rm erg \ s^{-1}})$	$6.99^{+0.0053}_{-0.0051}$	$6.98^{+0.0042}_{-0.0040}$	$6.77^{+0.0044}_{-0.0045}$	$7.23^{+0.0068}_{-0.0068}$	$6.43^{+0.0068}_{-0.0067}$
Goodness of fit	0.0001	0.0010	0.00 10	5.5000	3.0007
χ^2_{ν}	1.037	1.089	1.087	0.986	1.023

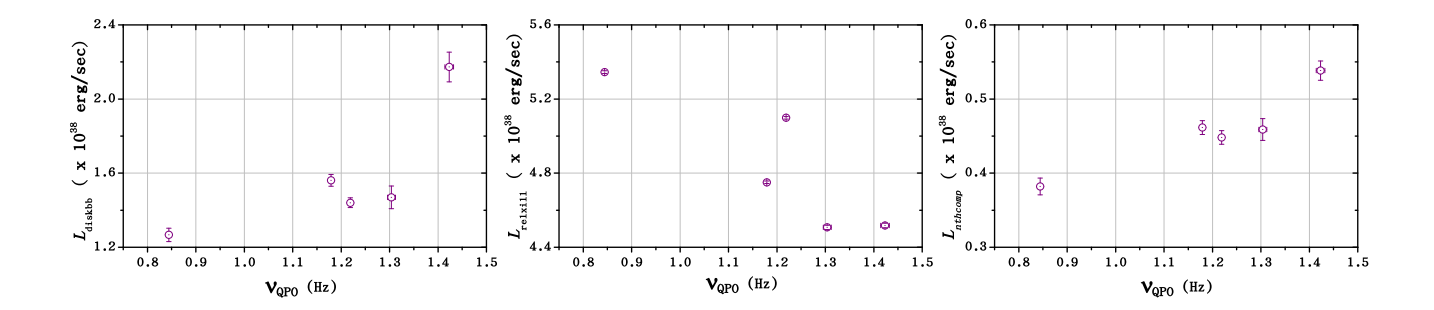


Figure 10: Unabsorbed 0.1100 keV luminosity components vs Type-C QPO ($\nu_{\rm QPO}$) assuming a source distance of D=3.7 kpc.

ing flow becomes radially more compact and globally more coherent, maximizing Q at an intermediate radius. Beyond this optimum, the transition region between hot flow and truncated disk becomes narrow, viscous coupling and magnetic instabilities strengthen, and phase mixing of the precessing structure increases, broadening the QPO and degrading coherence. Moreover, the coronal height and beaming pattern evolve during this shrinking, modifying the geometric attenuation of the modulated signal and contributing to the observed Q decline (Ingram et al., 2023). That Q also peaks at intermediate L (right panel, Fig. 4) reinforces the connection between coherence and accretion-geometry configuration. At lower L, the extended hot flow experiences greater propagating noise and stochastic fluctuations from the outer regions, degrading coherence; at higher L, enhanced disk-corona coupling and increased Compton cooling introduce nonlinear damping in the precessing structure. Thus, the optimal Q at intermediate L and v_{QPO} reflects an accretion state in which deterministic geometric modulation temporarily dominates over stochasticity and damping.

The tight correlation between Γ and ν_{OPO} (Deming fit showing $r \sim 0.95$; recall Fig. 9) further solidifies the link between truncation-radius evolution and timing properties. Specifically, the monotonic rise of ν_{QPO} from ~ 0.84 to ~ 1.45 Hz parallels progressive spectral softening, providing independent confirmation of inward truncation-radius motion (Ingram et al., 2009; Ingram and Done, 2011; Ma et al., 2025). In simple orderof-magnitude estimates, the observed 0.8-1.5 Hz frequencies, combined with estimates of black-hole mass $(M \sim 8-12 M_{\odot})$ and spin ($a_* = 0.98$), correspond to precessing-flow outer radii $r_{\rm out} \sim 16-21 \, r_{\rm g}$ (Ingram et al., 2009). As $v_{\rm OPO}$ climbs, the truncation radius must contract inward, bringing higher-density, cooler disk seed photons into the corona, thereby amplifying Compton losses and steepening Γ . This coordinated softeningwith-frequency motion is the hallmark signature of a truncateddisk/hot-flow system in which geometry and luminosity jointly regulate the spectral-timing behavior, and has been robustly documented in other transients (GX 339-4, MAXI J1535-571) during hard-intermediate states (Fürst et al., 2016; Yang et al., 2024).

Figure 10 shows the unabsorbed 0.1–100 keV component luminosities, L_{diskbb} , L_{relxill} , and L_{nthComp} , versus the QPO cen-

troid frequency v_{QPO} . The three components display distinct, coupled trends: L_{diskbb} and L_{nthComp} increase as v_{QPO} rises, whereas L_{relxill} declines across the same frequency range. This triad of $L(\nu_{OPO})$ behaviors quantitatively signals inward motion of the truncation radius and a precession-driven change in coronal geometry. As the truncation radius contracts, the thin disk extends deeper into the potential, raising its radiative efficiency and the supply of seed photons; the growth of $L_{\rm diskbb}$ therefore traces a larger effective emitting area at roughly constant color temperature. At the same time, the inner hot flow becomes more compact and dissipative, boosting the Compton power; the rise in L_{nthComp} and the associated softening of Γ reflect enhanced cooling of the corona by the strengthened disk photon field. Conversely, the shrinking truncation radius reduces the disk solid angle as seen by a precessing, mildly outflowing corona; anisotropic illumination then lowers the effective reflection fraction, producing the observed decrease in L_{relxill} . Altogether, this luminosity-space triad is consistent with global Lense-Thirring precession of a dynamical inner hot flow, wherein geometric reconfiguration modulates the energy partition between disk, corona, and reflection.

In conclusion, Swift J1727.8-1613's 2023 outburst provides an unprecedented opportunity to probe the inner-accretion-flow geometry and dynamics of a rapidly spinning black hole during a luminous hard-intermediate state. Our five coordinated NuSTAR observations reveal a coherent, multi-faceted picture of truncation-radius evolution driven by accretion-rate changes. The non-monotonic turnover in QPO coherence versus both frequency and luminosity directly constrains the operating regime of Lense-Thirring precession, demonstrating that geometric efficiency peaks at intermediate truncation radius before damping dominates at higher frequency. The tight correlation between photon index and QPO frequency (r = 0.95), coupled with the triadic luminosity evolution of disk, reflection, and Comptonization, provides robust, quantitative support for global precession of a dynamical inner hot flow. The apparentarea interpretation of disk-normalization variability, combined with stable cool-disk temperatures, sidesteps degeneracies in reflection-model fits and refines our understanding of colorcorrection and boundary-layer physics. Together, these results establish Swift J1727.8-1613 as a benchmark source for testing truncation-radius and LT-precession physics in black hole binaries, validating the paradigm of accretion-geometry control over timing and spectral properties during state transitions.

6. Data Availability

The data utilized in this study is available to the public through the HEASARC data archive, allowing for research purposes.

Acknowledgements

This study makes use of data obtained from the publicly accessible NASA HEASARC archive. The NuSTAR observations were sourced through the High Energy Astrophysics Science Archive Research Center (HEASARC) at NASAs Goddard Space Flight Center. We sincerely acknowledge the IUCAA Centre for Astronomy Research and Development (ICARD) and the Department of Physics, North Bengal University, for extending their research facilities. The authors also wish to thank the anonymous reviewer for constructive suggestions that significantly improved the clarity and quality of this manuscript. MT acknowledges CSIR, India for the research grant 161-411-3508/2K23/1. Authors (MG, NS, BCP) would like to acknowledge IUCAA, Pune for hospitality during a visit where the work is finalized. The authors thank Prof. Ranjeev Misra & Suchismito Chattopadhyay, IUCAA, Pune for fruitful discussions and support.

References

- Arnaud, K.A., 1996. Xspec: The first ten years, in: Jacoby, G.H., Barnes, J. (Eds.), ADASS V, p. 17.
- Bollemeijer, N., Uttley, P., You, B., 2025. A broad-band spectral-timing study of qpos in the bright black hole x-ray binary swift j1727. 8- 1613. Monthly Notices of the Royal Astronomical Society 540, 1394–1411.
- Bouchet, T., Rodriguez, J., Cangemi, F., Thalhammer, P., Laurent, P., Grinberg, V., Wilms, J., Pottschmidt, K., 2024. Integral/ibis polarization detection in the hard and soft intermediate states of swift j1727. 8- 1613. Astronomy & Astrophysics 688, L5.
- Brigitte, M., Segura, N.C., García, F., Svoboda, J., Trigo, M.D., Méndez, M., Vincentelli, F., Buisson, D.J., Altamirano, D., 2025. Detection of a type-c qpo during the soft-to-hard transition in swift j1727. 8-1613. arXiv preprint arXiv:2505.07938.
- Brigitte, M., Svoboda, J., 2025. X-ray polarization of accreting black holes: Cyg x-1 and swift j1727. 8-1613. arXiv preprint arXiv:2504.10981.

- Burridge, B.J., Miller-Jones, J.C., Bahramian, A., Prabu, S.R., Streeter, R., Segura, N.C., Santana, J.M.C., Knigge, C., Tremou, E., Carotenuto, F., et al., 2025. On the distance to the black hole x-ray binary swift j1727. 8–1613. arXiv preprint arXiv:2502.06448.
- Cao, H., Yang, J., Frey, S., Wood, C.M., Miller-Jones, J.C., Gabányi, K.É., Migliori, G., Giroletti, M., Cui, L., An, T., et al., 2025a. An ejection event captured by very long baseline interferometry during the outburst of swift j1727. 8–1613. The Astrophysical Journal Letters 987, L14.
- Cao, J.Y., Liao, J.Y., Zhang, S.N., Feng, H., Qu, J.L., Zhang, L., Liu, H.X., Yu, W., Zhao, Q.C., Peng, J.Q., et al., 2025b. Spectral analysis of the x-ray flares in the 2023 outburst of the new black binary transient swift j1727. 8–1613 observed with insight-hxmt. The Astrophysical Journal 983, 23.
- Casella, P., Belloni, T., Stella, L., 2005. The abc of low-frequency quasi-periodic oscillations in black hole candidates. The Astrophysical Journal 629, 403–407. URL: https://doi.org/10.1086/431174, doi:10.1086/431174.
- Debnath, D., Chang, H.K., Nath, S.K., Titarchuk, L., 2025. Evolution of qpo during rising phase of discovery outburst of swift j1727. 8-1613: Estimation of mass from spectrotemporal study. arXiv preprint arXiv:2504.16391.
- Debnath, D., Nath, S.K., Chatterjee, D., Chatterjee, K., Chang, H.K., 2024. Detection of qpo soft lag during the outburst of swift j1727. 8-1613: Estimation of intrinsic parameters from spectral study. The Astrophysical Journal 975, 194.
- Draghis, P.A., Miller, J.M., Homan, J., Uttley, P., Bollemeijer, N., Steiner, J.F., Hare, J., Tombesi, F., Gendreau, K.C., Arzoumanian, Z., et al., 2023. Preliminary spectral fitting and qpo evolution in nicer observations of black hole candidate swift j1727. 8-1613. The Astronomer's Telegram 16219, 1.
- Ewing, M., Parra, M., Mastroserio, G., Veledina, A., Ingram, A., Dovčiak, M., García, J.A., Russell, T.D., Baglio, M.C., Poutanen, J., et al., 2025. The very high x-ray polarisation of accreting black hole igr j17091- 3624 in the hard state. Monthly Notices of the Royal Astronomical Society, staf859.
- Fürst, F., Nowak, M.A., Tomsick, J.A., et al., 2016. A nustar spectrotiming study of gx 3394 in a hardintermediate state. The Astrophysical Journal 828, 34. doi:10.3847/0004-637X/828/1/34.
- Hughes, A., Carotenuto, F., Russell, T., Tetarenko, A., Miller-Jones, J., Plotkin, R., Bahramian, A., Bright, J., Cowie, F., Crook-Mansour, J., et al., 2025a. The peculiar hard state behaviour of the black hole x-ray binary swift j1727. 8–1613. arXiv preprint arXiv:2506.12387.
- Hughes, A.K., Carotenuto, F., Russell, T.D., Tetarenko, A.J., Miller-Jones, J.C., Bahramian, A., Bright, J.S., Cowie, F.J.,

- Fender, R., Gurwell, M.A., et al., 2025b. Comprehensive radio monitoring of the black hole x-ray binary swift j1727. 8–1613 during its 2023–2024 outburst. arXiv preprint arXiv:2506.07798.
- Ingram, A., Done, C., 2011. A physical model for the continuum variability and quasi-periodic oscillation in accreting black holes. Monthly Notices of the Royal Astronomical Society 415, 2323–2335. doi:10.1111/j.1365-2966.2011. 18860.x.
- Ingram, A., Done, C., Fragile, P.C., 2009. Low-frequency qpos and lense-thirring precession. MNRAS 397, L101–L105.
- Ingram, A., Veledina, A., Poutanen, J., et al., 2023. Tracking the x-ray polarization of the black hole transient swift j1727.8–1613 during a state transition. arXiv:2311.05497.
- Ingram, A.R., van der Klis, M., 2017. On the different flavours of lensethirring precession around accreting black holes. Monthly Notices of the Royal Astronomical Society 473, 431–439. doi:10.1093/mnras/stx2357.
- Ingram, A.R., Motta, S.E., 2019. A review of quasi-periodic oscillations from black hole x-ray binaries: observation and theory. New Astronomy Reviews 85, 101524.
- Ingram, A.R., Motta, S.E., 2020. A review of quasiperiodic oscillations from black hole x-ray binaries: observation and theory. New Astronomy Reviews 85, 101524. URL: https://doi.org/10.1016/j.newar. 2020.101524, doi:10.1016/j.newar.2020.101524.
- Jin, P., Méndez, M., García, F., Altamirano, D., Zhang, G., Rout, S.K., 2025. Timing analysis of the black hole candidate swift j1727. 8–1613: Detection of a dip-like feature in the high-energy cross spectrum. Astronomy & Astrophysics 699, A9.
- Liao, J., Chang, N., Cui, L., Jiang, P., Mou, D., Huang, Y., An, T., Ho, L.C., Feng, H., Fu, Y.C., et al., 2025. Tracking the jet-like corona of black hole swift j1727. 8- 1613 during a flare state through type-c quasiperiodic oscillations.
- Liu, H.X., Xu, Y.J., Zhang, S.N., et al., 2024. The broadband x-ray spectral properties during the rising phases of the outburst of swift j1727.8–1613. arXiv arXiv:2406.03834.
- Ma, R., Done, C., Kubota, A., 2025. Testing the lensethirring precession origin of the qpo in swift j1727.81613. Monthly Notices of the Royal Astronomical Society doi:10.48550/arXiv.2506.18857. in press; arXiv:2506.18857.
- Majumder, S., Kushwaha, A., Singh, S., Jayasurya, K.M., Das, S., Nandi, A., 2025. Probing the accretion geometry of black hole x-ray binaries: A multi-mission spectro-polarimetric and timing study. arXiv preprint arXiv:2506.03774.
- Mata Sánchez, D., Torres, M.A.P., Casares, J., Muñoz-Darias, T., Armas Padilla, M., Yanes-Rizo, I.V., 2024. Dynamical confirmation of a black hole in the x-ray transient swift

- j1727.8–1613. arXiv e-prints URL: https://arxiv.org/abs/2408.13310. submitted to A&A; use arXiv until final pagination.
- Mereminskiy, I., Lutovinov, A., Molkov, S., Krivonos, R., Semena, A., Sazonov, S., Tkachenko, A., Sunyaev, R., 2024. Hard x-rays and qpo in swift j1727.8–1613: the rise and plateau of the 2023 outburst. MNRAS 531, 4893–4899.
- Nandi, A., Das, S., Majumder, S., Katoch, T., Antia, H., Shah, P., 2024. Discovery of evolving low-frequency qpos in hard x-rays (100 kev) observed in black hole swift j1727. 8-1613 with astrosat. Monthly Notices of the Royal Astronomical Society 531, 1149–1157.
- Peng, J.Q., Zhang, S., Shui, Q.C., Zhang, S.N., Chen, Y.P.,
 2025. A possible jet and corona configuration for swift j1727.
 8–1613 during the hard state. Journal of High Energy Astrophysics 45, 316–324.
- Peng, J.Q., Zhang, S.N., Qu, J.L., et al., 2024. Nicer, nustar, and insight-hxmt views to swift j1727.8–1613. ApJ Letters 960, L17.
- Podgorný, J., Svoboda, J., Dovciak, M., Veledina, A., Poutanen, J., et al., 2024a. Recovery of the x-ray polarisation of swift j1727.8–1613 after the soft-to-hard transition. A&A 687, A28.
- Podgorný, J., Svoboda, J., Dovčiak, M., Veledina, A., Poutanen, J., et al., 2024b. Recovery of the x-ray polarisation of swift j1727.8–1613 after the soft-to-hard spectral transition. Astronomy & Astrophysics 687, A28. doi:10.1051/0004--6361/202450566.
- Podgorný, J., Svoboda, J., Dovčiak, M., et al., 2024c. Recovery of the x-ray polarisation of Swift J1727.8-1613 after the soft-to-hard spectral transition. A&A 686, L12. arXiv:2404.19601.
- Rawat, D., Méndez, M., García, F., Maggi, P., 2025. Evolution of the comptonizing medium of the black-hole candidate swift j1727. 8–1613 along the hard to hard-intermediate state transition using nicer. Astronomy & Astrophysics 697, A229.
- Shui, Q.C., Zhang, S., Peng, J.Q., Zhang, S.N., Chen, Y.P., Ji, L., Kong, L.D., Feng, H., Yu, Z.L., Wang, P.J., et al., 2024. Phase-resolved spectroscopy of low-frequency quasiperiodic oscillations from the newly discovered black hole x-ray binary swift j1727. 8-1613. The Astrophysical Journal 973, 59.
- Stiele, H., Kong, A.K.H., 2024. Nicer and swift/xrt monitoring of the 2023 outburst of swift j1727.8–1613. A&A In press.
- Titarchuk, L., Soffitta, P., Seifina, E., Muleri, F., Mikusincova, R., 2025. X-ray linear polarization prediction in black-hole binaries and active galactic nuclei and its measurements by ixpe. arXiv preprint arXiv:2506.09571.

- Veledina, A., et al., 2023. Discovery of x-ray polarization from the black hole transient swift j1727.8–1613. The Astrophysical Journal Letters 958, L16. doi:10.3847/2041--8213/ad0781.
- Wilms, J., Allen, A., McCray, R., 2000. On the absorption of x-rays in the interstellar medium. ApJ 542, 914–924.
- Wood, C.M., Miller-Jones, J.C.A., Bahramian, A., et al., 2024. Swift j1727.8–1613 has the largest resolved continuous jet ever seen in an x-ray binary. arXiv e-prints URL: https://arxiv.org/abs/2405.12370.
- Yang, Z.X., Zhang, L., Zhang, S.N., et al., 2024. A timing view of the additional high-energy spectral component in swift j1727.8–1613. arXiv:2407.05236.
- Yu, W., Bu, Q.C., Zhang, S.N., et al., 2024. Timing analysis of the newly discovered black hole candidate swift j1727.8–1613 with insight-hxmt. MNRAS 529, 4624–4632.
- Zdziarski, A.A., Wood, C.M., Carotenuto, F., 2025. A novel method of modeling extended emission of compact jets: Application to swift j1727. 8- 1613. The Astrophysical Journal Letters 986, L35.
- Zhao, Q.C., Tao, L., Li, H.C., Zhang, S.N., Feng, H., Ge, M.Y., Ji, L., Wang, Y.N., Huang, Y., Ma, X., et al., 2024. The first polarimetric view on quasiperiodic oscillations in a black hole x-ray binary. The Astrophysical Journal Letters 961, L42.
- Zhou, J., Huang, J., Chang, X., Okuda, T., Singh, C.B., 2025. Numerical studies of (in) stabilities of shocks in perturbed advective flows around black holes. Journal of High Energy Astrophysics, 100395.